Applicability of the critical state model to small ceramic Y–Ba–Cu–O particles in low magnetic fields

E. V. Blinov, Yu. P. Stepanov, K. B. Traito, and L. S. Vlasenko

A. F. Ioffe Physico-Technical Institute, Academy of Sciences of Russia, 194021 St. Petersburg, Russia

R. Laiho and E. Lähderanta

Wihuri Physical Laboratory, University of Turku, 20500 Turku, Finland

Dependence of the isothermoremanent magnetization M_{IR} on the magnetizing field H_0 has been investigated in ceramic Y–Ba–Cu–O samples with different size of particles. It is shown that when the particles have dimensions less than 200 μm, the critical state model can be applied for the description of the trapped magnetic flux in low magnetic fields only with an additional assumption that a vortex-free region exists near the surface of the particles.

1. INTRODUCTION

Many properties of metal-oxide high-T_c superconductors depend on the size of the sample. For ceramic materials the influence of the sample size on the transport critical current density[1–4] and size dependence of the AC susceptibility[4–6] have been investigated. In powdered Y–Ba–Cu–O with particle size of the order of several μm, the quantum dimensional effect has been observed[7] and size dependence of high-frequency power absorption has been studied.[8] It was shown also[9] that for particles smaller than the field penetration length, the threshold field for formation and trapping of a vortex when the sample is cooled in a magnetic field (FC) and in zero field (ZFC) depends on the particle size.

It is well known that the magnetic flux structure in ceramic high-T_c superconductors is a complex question. In these materials, magnetic flux vortices can be divided into two groups: intergrain and intragrain. When the field is increased, starting from zero, the intergrain vortices penetrating the weak-link network can become trapped there in fields $H > H_{c1}^w$, where H_{c1}^w is the first critical field of the weak links.[10,11] When the first critical field of the grains H_{c1} is exceeded, fluxons enter the grains.

It was shown[12–14] that comparison of the isothermoremanent magnetization M_{IR} for ceramics and powders enables us to distinguish between the behavior of inter- and intragrain vortices and to find a range of magnetizing fields H_0 where the remanent magnetization of the ceramic sample can be attributed only to the intergrain vortices.

In the present paper, the behavior of the M_{IR} attributed to intergrain vortices is investigated for Y–Ba–Cu–O ceramics with particle sizes in the range 10–250 μm. It is demonstrated that the dependence of the remanent magnetization on H_0 predicted by the critical state model disagrees with experimental results for ceramic particles smaller than 200 μm. This result can be explained by the existence of a vortex-free region near the surface.

2. EXPERIMENTAL

The basic ceramic material was prepared from sintered pellets of Y–Ba–Cu–O annealed for 5 h at 940 °C, 20 h at 906 °C and for 10 h at 400 °C. As a result of this treatment the grain size of the ceramic was 5–10 μm. After crushing this material the particles were separated into four groups with sizes 130–260 μm, 100–130 μm, 60–75 μm and 10–60 μm, respectively. The samples (1–4) used in this work were prepared from these four groups of powders so that the total mass of each sample was 40 mg. The quantity of the nonsuperconducting phase in the samples was investigated by examining their electron paramagnetic resonance (EPR) spectra.

The magnetic investigations were carried out with an rf-SQUID magnetometer. Values of M_{IR} were determined as follows. After warming the sample to some temperature above 130 K, it was cooled in zero magnetic field down to 77 K. Then the magnetizing field H_0 was applied. After switching off H_0, M_{IR} was measured by passing the sample through a pair of counterwound pick-up coils connected on the SQUID.

3. EXPERIMENTAL RESULTS AND DISCUSSION

In Fig. 1, the dependence of the isothermoremanent magnetization M_{IR} on H_0 is presented for the basic ceramic material consisting of particles longer than 260 μm. The analysis made by distinguishing the behavior of inter- and intragrain vortices, as described in[12–14] shows that when H_0 rises to 7 Oe, the increase in M_{IR} corresponds mainly to intergrain vortices trapped in the weak links. The increase in magnetization in higher fields ($H_0 > 10$ Oe) is due to magnetic flux trapped in the grains.

Figure 2 shows the dependance of M_{IR} on H_0 for samples 1–4 which have differing particle sizes. As can be seen for fields higher than 150 Oe, where the magnetization M_{IR} is saturated, the peak value of $M_{IR\,sat}$ is lower for samples 3 and 4 than for samples 1 and 2, and it decreases with decreasing particle size.

As was shown in[15,16] EPR measurements on polycrystalline Y–Ba–Cu–O materials can be used to estimate the quantity of the nonsuperconducting phase in high-T_c superconductors. Indeed, EPR investigations carried out for our samples 1–4 showed that the decrease in $M_{IR\,sat}$ in speci-
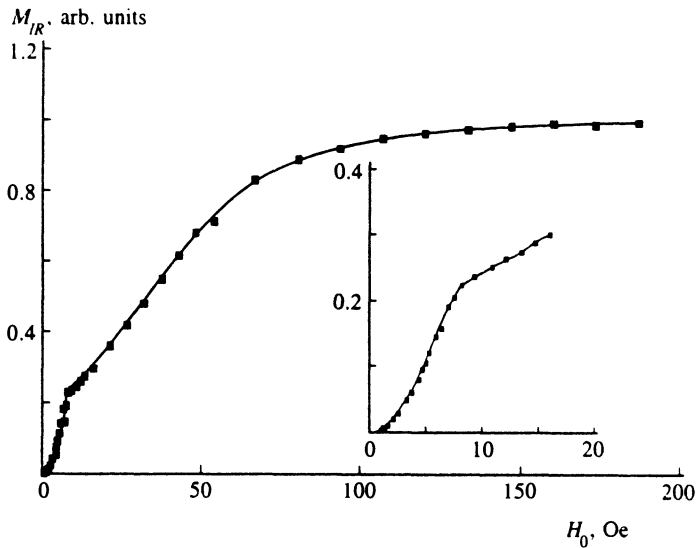
1063-7761/94/090433-06$10.00

FIG. 1. Dependence of isothermoremanent magnetization M_{IR} on the field H_0 for the basic ceramic material consisting of particle larger than 260 μm.

mens 3 and 4 is due to an increase in the nonsuperconducting phase. Taking into account the variation in the amount of the superconducting phase in the samples, the dependence of M_{IR} on H_0 has been normalized in the saturation region.

This result indicates that the procedure of crushing the basic ceramic material to prepare small particles results in destroying the surface layer of the particle. It is easy to estimate that a 2–3 μm thick surface layer can be responsible for the observed increase in the nonsuperconducting phase (see Fig. 2). Thus, the size of the superconducting part of the particle becomes less than real geometrical size. This effect should be taken into account in experiments where the relationship between particle size and penetration length is important.[9,17]

Figure 3 shows the behavior of the remanent magnetization of samples 1–4 (curves 1–4) in the low magnetic field region where intergrain vortices start to penetrate the sample. It appears that the value of the magnetization corresponding to saturation of the weak link network is not very sharply

defined, because intragrain vortices are already trapped in the grains in magnetic fields as low as 10 Oe. Nevertheless we can estimate the values of M_{sat1}, M_{sat2}, and M_{sat2} corresponding to saturation of the weak links in samples 1, 2, and 3 (see Fig. 3). In fact, the magnetization of sample 4, with particle size 10–60 μm, does not reveal the intergranular magnetization.

Let us assume that only one kind of vortex penetrates a cylindrical sample of radius R. If the size of the vortices is less than that of the sample, a spatial distribution of trapped flux should be realized. Taking the standard approach,[18–19] which takes only irreversible current arising from vortex into pinning into account, one can find the profile of the field inside the sample using the critical state equation.

$$\text{curl } B(r) = \pm \frac{4\pi}{c} J_c(B) \qquad (1)$$

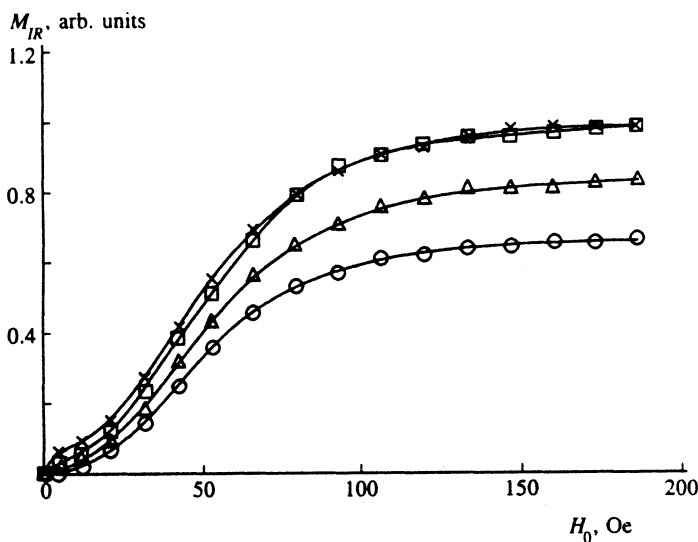with boundary condition $B(0) = 0$. Here J_c is the critical

FIG. 2. Dependence of M_{IR} on H_0 in the range of 0–200 Oe for samples 1–4 with ceramic particle sizes 130–260 μm (crosses), 100–130 μm (squares), 60–75 μm (triangles), and 10–60 μm (circles), respectively.

M_{IR}, norm. units

current and B is the magnetic inductance, which is equal to $n\Phi_0$ (n is the vortex density and Φ_0 is the magnetic flux quantum). The signs (+) and (−) correspond to decreasing and increasing field profiles inside the sample, respectively. In this case the isothermoremanent magnetization is

$$M_{IR} = \frac{1}{2}\,\frac{\mu}{V}\int_0^R B(r)\,r\,dr,\qquad(2)$$

where V is the volume of the sample and μ is the effective magnetic permeability, taking into account the screening of the grains (if the London penetration depth λ_L is less than the grain size d_g, $\mu \approx \lambda_L d_g$; if $\lambda_L \geq d_g$, $\mu \approx 1$.) For the calculations, we use a critical current of the form $J_c = J_{c0}[1 + (B/B_0)^2]^{-1}$, where J_{c0} is the critical current density at $B = 0$ and B_0 is a parameter. This kind of expression is known to be valid in ceramic high-T_c materials.[2,3,20,21]

Figure 4 shows the theoretical dependence of M_{IR} on H_0 for a unit mass of cylindrical samples with different radii: R_1 (curve 1), R_2 (curve 2), and R_3 (curve 3). We used in our calculations the ratios of the radii as $R_2/R_1 = 0.59$ and $R_3/R_1 = 0.36$, selected according to the average radius of samples 1–3. As can be seen from Fig. 4, the saturation value of the magnetization decreases with decreasing radius. Furthermore, a crossing of the curves is observed. Thus, at very low magnetic fields the samples with smaller radius have higher magnetization. This behavior of M_{IR} is illustrated in Figs. 5 and 6, where the simplest case of an infinite slab in a magnetic field parallel to its surface is considered. In Fig. 5 the spatial distribution of the flux through the sample corresponding to saturation, has been presented for a

slab of thickness d (Fig. 5a) and for two slabs of thicknesses $d/2$ (Fig. 5b). It is clear from this figure that the total trapped magnetic flux is proportional to the area under the curve. This area decreases with decreasing slab thickness (for slabs of thickness $d/2$, it is less than for the slab of thickness d). In Figs. 6a and 6b, the spatial distribution of the flux in the
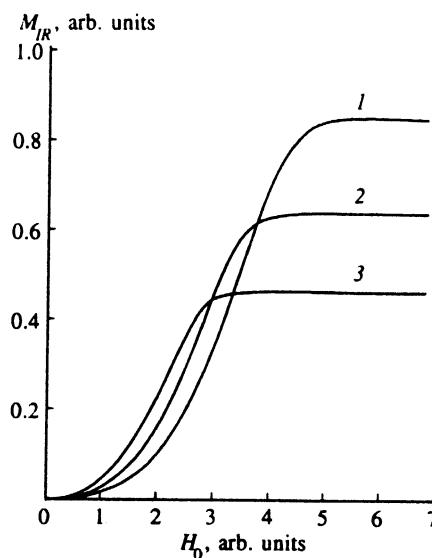

M_{IR}, arb. units

H_0, arb. units

FIG. 4. Theoretical dependence of M_{IR} on H_0 for cylindrical samples with different radii: R_1 (curve 1), R_2 (curve 2), and R_3 (curve 3). The ratios of the radii are $R_2/R_1 = 0.59$ and $R_3/R_1 = 0.36$. M_{IR} and H_0 are normalized by the parameter B_0.
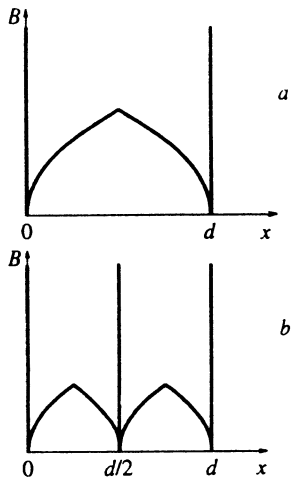
FIG. 5. Schematic profile of the peak trapped magnetic flux calculated in the framework of the critical state model for slabs with an infinite a- and b-axis and finite thickness; a) one slab with thickness d; b) two slabs with thickness $d/2$. The field is parallel to the plane of the slabs.

same samples is shown for $H_0 < H^*$, where H^* is the lowest magnetic field at which the penetrating flux reaches the center of the sample. If $H_0 < H^*$ in the smallest sample, as shown in Fig. 6b, the total magnetic moment for the two slabs will be higher than for the thick one. Similar considerations for samples with other shapes lead to a qualitatively similar result: in a low magnetic field, smaller samples have higher magnetization, but in the region of saturation smaller samples have lower magnetization.

Nevertheless, as was shown in Fig. 3 for samples with particle size less than 200 μm, no crossing of the M_{IR} vs H_0 curves is observed. This disagreement with the theoretical

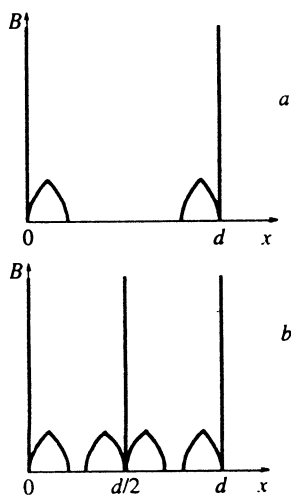
FIG. 6. Schematic profile of the trapped magnetic flux calculated in the framework of the critical state model for slabs with an infinite a- and b-axis and finite thickness; a) one slab with thickness d; b) two slabs with thickness $d/2$. The field H_0 is parallel to the plane of the slab. $H_0 < H^*$, where H^* is the lowest magnetic field at which the penetrating flux reaches the center of the sample with the smaller thickness.
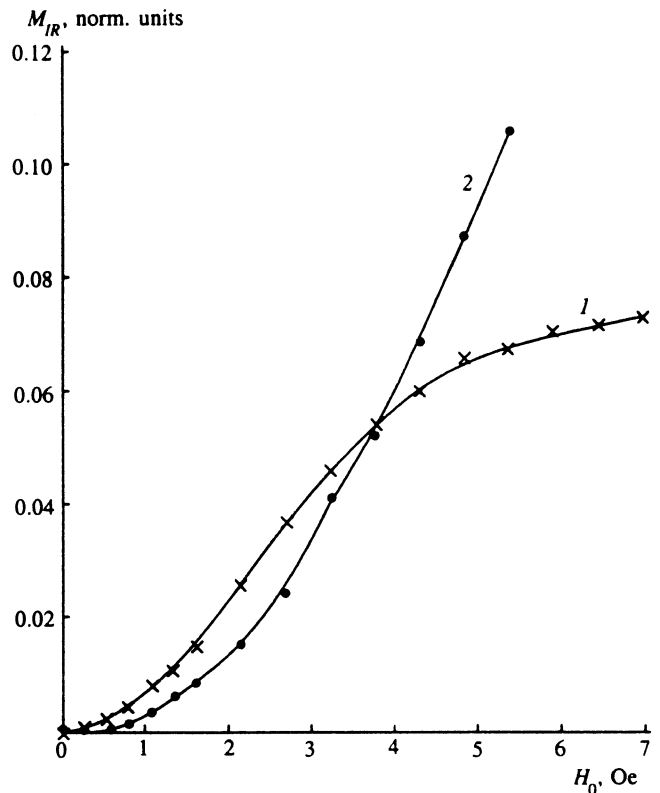

FIG. 7. Dependence of M_{IR} on H_{-0} in the range 0–7 Oe; 1) sample 1 (particle size 130–260 μm); 2)—sample containing pieces of the basic material (particle size >260 μm).

prediction (see Fig. 4) indicates that in these particles the actual profile of the trapped magnetic flux differs from that described above and shown in Fig. 6.

To estimate the size of the ceramic particles required for the spatial distribution of the flux shown in Fig. 6b, we have compared M_{IR} for sample 1 (particle size 130–260 μm) and for a sample containing pieces of the basic material (particle size >260 μm). As can be seen from Fig. 7, M_{IR} of sample 1 is up to $H_0 = 3.8$ Oe higher than M_{IR} of the sample consisting of particles with size >260 μm. We can therefore conclude that the spatial distribution of the flux can be described by the critical state model in our ceramics only for particles larger than 250 μm). For smaller particles a more detailed examination of the field distribution should be carried out.

Indeed, in the case of remanent magnetization, the induction B is zero at the surface of the particle and has a very low value in the surface layer. According to Ref. 22, equilibrium currents associated with the diamagnetism of the vortex lattice should then be taken into account. A critical state model based on this approach has been developed for an Abrikosov vortex lattice.[22-24] As will be shown below, taking equilibrium into account implies that a vortex-free region should exist near the surface.

For isothermoremanent magnetization, the distribution of the vortex density $n = B/\Phi_0$ can be obtained from the equations

$$\text{curl } H(B) = \pm \frac{4\pi}{c} J_c(H),\qquad(3)$$

$$H = H_{eq}(B),\qquad(4)$$

with the boundary condition

$$H(0) = 0.\qquad(5)$$

Here $H(B)$ is the thermodynamic field, $H_{eq}(B)$ is the dependence of this field H on B, and $H(0)$ is the value of the thermodynamic field at the surface.

Let us consider the same extended critical state model for the weak link network. The structure of the intergranular vortex lattice has been analyzed in many papers (see, e.g., Refs. 25–29). It has been shown that in low-density ceramics, a low magnetic field penetrates weak links in the form of hypervortices.[27] In higher fields, Josephson vortices are formed.[28] For a low density ceramic with a weak critical current, as considered here, it is reasonable to suggest that the grain size is less than the Josephson penetration depth and the hypervortex lattice is realized in a low magnetic field. Then the effective medium theory can be used,[27,28] and the magnetization curve can be approximated by the formula for an Abrikosov vortex lattice with the parameter renormalization $H_{c1} \rightarrow H_{c1}^w, \lambda_L \rightarrow \delta$. Here H_{c1} is the lower critical field for the Abrikosov vortices, $H > H_{c1}^w$ is the critical field for penetration of the hypervortices, λ_L is the London penetration depth and δ is the effective penetration depth for the weak-link network. Using the Dunn–Hlawiczka formula,[30] which can be applied to the Abrikosov vortex lattice as shown in paper,[31] we can obtain the function $H_{eq}(B)$

$$H = B + H_{c1}^w.\qquad(6)$$

Analysis of Eqs. (3), (4), and (6) shows that the field profiles given in Figs. 5 and 6 do not satisfy the boundary condition (5) since for $B \rightarrow 0$ one can obtain from Eq. (6) that $H \rightarrow H_{c1}^w$, i.e., $H_{in}(x \rightarrow 0) \rightarrow H_{c1}^w$ and $H(0) \neq 0$. It means that discontinuity of the thermodynamic potential appear at the border, i.e., infinite expulsion forces affect the surface vortices. The expulsion of the surface vortices result in the formation of a vortex-free region (where $B = 0$).

The existence of a vortex-free region has been considered by J. R. Clem[32] for description of a mixed state structure in an external field and without bulk pinning. He showed that its width, x_f, depends on the external field H_{ex} and on the magnetic induction B inside the sample. In a dense vortex lattice x_f is approximately equal to the intervortex distance. The concept of vortex-free region is important for description of relaxation experiments[33] and calculation of a.c. response.[34]

For remanent magnetization, the width x_f of the vortex-free region can be obtained as follows. Inside the vortex-free region, H obeys the London equation

$$H - \delta^2 \frac{\partial^2 H}{\partial x^2} = 0\qquad(7)$$

with the continuity conditions for the current and the field at the boundaries of the vortex-free region
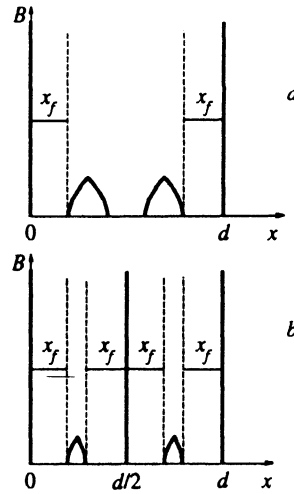
$$J(xf) = J_c,\qquad(8)$$

FIG. 8. Schematic profile of the trapped magnetic flux calculated in the framework of the extended critical state model for slabs with an infinite a- and b-axis and finite thickness; a) one slab with thickness d; b) two slabs with thickness $d/2$. The field H_0 is parallel to the plane of the slab. $H_0 < H^{**}$, where H^{**} is the lowest magnetic field at which the penetrating flux reaches the center of the sample with the bigger thickness. x_f is the vortex-free region.

$$H(0) = 0,\qquad(9)$$

$$H(x_f) = H_{c1}^w.\qquad(10)$$

The last condition is obtained from Eq. (6).

From Eqs. (7)–(10) we find the equation for x_f,

$$\frac{H_{c1}^w}{\delta} \coth \frac{x_f}{\delta} = \frac{4\pi}{c} J_c.\qquad(11)$$

Let us assume the value x_f. As was shown in Ref. 27

$$H_{c1}^w = \frac{2\pi}{c} J_0 d_g \ln \frac{\delta}{d_g}.\qquad(12)$$

The calculation of the pinning energy for the intergranular vortex carried out in Ref. 25 enables us to obtain

$$J_c \approx \frac{J_0}{5}.\qquad(13)$$

In Eqs. (12), (13) J_0 is the density of the current through Josephson junction.

If $\delta \gg d_g$, x_f we get

$$x_f \frac{5}{2} d_g \ln \frac{\delta}{d_g}.\qquad(14)$$

Thus, for our ceramic x_f can be estimated to be 30 μm.

As a result, instead of the profile shown in Fig. 6, the distribution of B shown in Fig. 8 is realized. From this figure it can be seen that if the distance between the two parts of the trapped profile inside the particle is less than $2x_f$, cutting the particle results in a decrease in the trapped magnetic moment. Thus the observed behavior of M_{IR} (Fig. 3) can be explained by the extended critical state model, taking into account the existence of the vortex-free region.

4. CONCLUSION

The influence of the size of the ceramic particles on the behavior of the isothermoremanent magnetization M_{IR} versus magnetizing field H_0 has been studied. For Y–Ba–Cu–O ceramics having particles in the range 10–250 μm, the trapped magnetic flux (per unit mass) attributed to the intergrain vortices decreases with particle size for all values of H_0. Such behavior contradicts the theoretical prediction based on the critical state model. To explain this disagreement, an extended critical state model that takes into account the existence of a vortex-free region near the surface of the particle has been developed for the weak-link network. This extended model should be used when the size of the vortex-free region becomes comparable to the size of the particles.

[1] H. Dersch and G. Blatter, Phys. Rev. **38**, 11391 (1988).

[2] A. A. Zhukov, V. V. Moschcalkov, D. A. Komarkov, V. P. Shabatin, A. A. Bush, S. N. Gordeev, D. V. Shelomov, Physica C **162–164**, 1623 (1989).

[3] K.-H. Müller, D. N. Matthews, and R. Driver, Physica C **191**, 339 (1992).

[4] V. Skumryev, M. R. Koblinschka, and H. Kronmüller, Physica C **184**, 332 (1991).

[5] M. Forsthuber, F. Ludwig, G. Hilscher, Physica C **177**, 401 (1991).

[6] M. Forsthuber, G. Hilscher, Phys. Rev. B **45**, 7996 (1992).

[7] V. Fleisher, E. Lähderanta, R. Laiho, and Yu. P. Stepanov, Physica C **170**, 161 (1990).

[8] M. M. Afanas'ev, E. V. Blinov, L. S. Vlasenko, M. P. Vlasenko, Yu. P. Stepanov, V. G. Fleisher, Pis'ma Zh. Eksp. Theor. Fiz. **51**, 529 (1990) [JETP Lett. **51**, 600 (1990)].

[9] E. V. Blinov, L. S. Vlasenko, Yu. A. Kufaev, E. B. Sonin, Yu. P. Stepanov, A. K. Tagantsev, and V. G. Fleisher, Zh. Eksp. Teor. Fiz. **103**, 617 (1993) [JETP **76**, 308 (1993)].

[10] B. Loegel, D. Bolmont, A. Mehdaoui, Physica C **159**, 816 (1989).

[11] R. Laiho, E. Lähderanta, L. Säisä, Gy. Kovács, G. Zsolt, I. Kirshner, and I. Halász, Phys. Rev. B **42**, 347 (1990).

[12] E. V. Blinov, E. Lähderanta, R. Laiho, Yu. P. Stepanov, Physica C **199**, 201 (1992).

[13] A. Shaulov, Y. Yeshurun, S. Shatz, R. Harenveni, Y. Wolfus, S. Reich, Phys. Rev. b **43**, 3760 (1991).

[14] V. Keith and H. J. T. Smith, Physica C **218**, 8 (1993).

[15] F. J. Owens, B. L. Ramakrishna, and Z. Iqbal, Physica C **156**, 221 (1988).

[16] D. K. De, J. Phys. C: Solid State Phys. **21**, 4481 (1988).

[17] E. Lähderanta, L. Vlasenko, and R. Laiho, Physica C **190**, 497 (1992).

[18] Ming Xu, Phys. Rev. B **44**, 2713 (1991).

[19] Ming Xu, A. Umezawa, and G. W. Crabtree, Phys. Rev. B **46**, 11928 (1992).

[20] L. M. Fisher, N. V. Il'in, N. A. Podlevskikh, and S. I. Zakharchenko, Solid State Commun. **73**, 687 (1990).

[21] E. V. Blinov, E. B. Sonin, A. K. Tagantsev, and K. B. Traito, Supercond. Phys. Chem. Technol. **4**, 426 (1991).

[22] J. Friedel, P.-G. de Gennes, and J. Matricon, Appl. Phys. Lett. **2**, 119 (1963).

[23] A. M. Campbell and J. E. Ivetts, Adv. Phys. **21**, 199 (1972).

[24] J. R. Clem and Z. Hao, Phys. Rev. B **48**, 13774 (1993).

[25] C. J. Lobb, D. W. Abraham, M. Tinkham, Phys. Rev. B **27**, 150 (1983).

[26] S. John and T. C. Lubensky, Phys. Rev. B **34**, 4185 (1986).

[27] E. B. Sonin, Pis'ma Zh. Eksp. Teor. Fiz. **47**, 415 (1988) [JETP Lett. **47**, 496 (1988)].

[28] E. B. Sonin, A. K. Tagantsev, Phys. Lett. A **140**, 127 (1989).

[29] V. V. Bryksin, S. N. Dorogovtsev, Zh. Eksp. Teor. Fiz. **102**, 1025 (1992) [Sov. Phys. JETP **75**, 558 (1992)].

[30] W. I. Dunn and P. Hlawiczka, J. Phys. D **1**, 1469 (1968).

[31] L. Burlachkov, Y. Yeshurun, M. Konczykowski, and F. Holtsberg, Phys. Rev. B **45** (1992).

[32] J. R. Clem, Low. Temp. Physics LT-13, H. D. Timmerhaus, W. J. O'Sillivan, and E. F. Hammel (eds)., Plenum, New York V. **3**, p. 102 (1974).

[33] L. Burlachkov, Phys. Rev. B **47**, 8056 (1993).

[34] E. B. Sonin and K. B. Traito, submitted to Phys. Rev. B.